Terahertz-field-induced Nonlinear Electron Delocalization in Au Nanostructures

Katsumasa Yoshioka,[†] Yasuo Minami,[,†] Ken-ichi Shudo,[†] Thang D. Dao,[‡,§] Tadaaki Nagao,[‡,§]*

Masahiro Kitajima,[†,‡,§,∥,⊥] Jun Takeda,[,†] and Ikufumi Katayama[*,†]*

†Department of Physics, Graduate School of Engineering, Yokohama National University,

Yokohama 240-8501, Japan

‡International Center for Materials Nanoarchitectonics, National Institute for Materials Science,

Tsukuba 305-0044, Japan

§CREST, Japan Science and Technology Agency, Kawaguchi 332-0012, Japan

∥LxRay Co. Ltd., Nishinomiya 663-8172, Japan

⊥Department of Applied Physics, National Defense Academy, Yokosuka 239-8686, Japan

Improved control over the electromagnetic properties of metal nanostructures is indispensable for the development of next-generation integrated nanocircuits and plasmonic devices. The use of terahertz (THz)-field-induced nonlinearity is a promising approach to controlling local electromagnetic properties. Here, we demonstrate how intense THz electric fields can be used to modulate electron delocalization in percolated gold (Au) nanostructures on a picosecond timescale. We prepared both isolated and percolated Au nanostructures deposited on high resistivity Si(100) substrates. With increasing the applied THz electric fields, large opacity in the THz transmission spectra takes place in the percolated nanostructures; the maximum THz-field-induced transmittance difference, 50% more, is reached just above the percolation threshold thickness. Fitting the experimental data to a Drude-Smith model, we found furthermore that the localization parameter and the damping constant strongly depend on the applied THz-field strength. These results show that ultrafast nonlinear electron delocalization proceeds via strong electric field of THz pulses; the intense THz electric field modulates the backscattering rate of localized electrons and induces electron tunneling between Au nanostructures across the narrow insulating bridges without any material breakdown.

Recently, the generation of high power terahertz (THz) waves with electric fields of 0.1–1 MV/cm has been achieved using ultrashort laser pulses.[1-6] In contrast with optical radiation, THz waves can not only access low-frequency atomic and molecular motions directly but can also accelerate conduction electrons without any interband excitation. Exploiting these advantages, non-thermal and nonlinear phenomena induced by intense THz electric field transients have been demonstrated in a wide range of materials, notably dielectrics,[7-9] semiconductors,[10-12] and semimetals.[13,14] However, notwithstanding their fascinating electromagnetic properties, very few studies have been devoted to metallic systems.

Among these, gold (Au) has been widely studied in the fields of microelectronics and bio-sensing because of its high conductivity and chemical stability. Ultrathin Au films can manifest unique electromagnetic properties that deviate strongly from those of the bulk material, depending on their morphologies; for example, an insulator-to-metal transition (IMT) induced by a percolating network,[15,16] huge surface plasmon-enhanced electric fields applicable to optical bio-sensing,[17] percolation-enhanced THz generation,[18] and quantum tunneling between Au grains.[19,20] Owing to these unique electromagnetic properties, Au nanostructures are promising candidates for a new class of integrated nanocircuits and plasmonic devices. In this context, improved control of Au nanostructures and of their electromagnetic properties in nanometer-scale are highly desirable.

To explain the dielectric properties of inhomogeneous metal nanostructures, effective-medium theories such as the Maxwell-Garnet[21] and Bruggeman[22] models have been proposed. However, these models struggle to describe systems with strong carrier localization arising from carrier backscattering at grain boundaries—this occurs when the grain size of the nanostructures becomes comparable to the mean free path of conduction electrons at the Fermi energy (e.g. 25–

35 nm in Au).[23] In such cases, a phenomenological Drude-Smith model is generally used to explain the carrier response of inhomogeneous metal nanostructures. This is an extension of the simple Drude model, that has only been applied however in narrow frequency windows.[16,23-28]

In the present study, large THz-field-induced opacity is demonstrated in Au nanostructures. The experimental THz transmissions and complex dielectric spectra are well described by the phenomenological Drude-Smith model over relatively broad frequency ranges of 0.35–1.25 THz and 13–100 THz. With increasing THz electric field strengths, the THz transmittance decreases dramatically in the percolated Au nanostructures, indicating that intense THz electric fields induce a unique nonlinear transportation of conduction electrons.

Ultrathin Au films with different average thicknesses were deposited on a 500 μm-thick high resistivity Si(100) wafer covered by a native oxide of about 2 nm thickness.[29] High-resistivity Si is used to avoid nonlinear effects from the substrate under intense THz irradiation.[14,30] All films were prepared by sputtering and without any post-annealing to obtain Au nanostructures that were both isolated and percolated. The surface morphology of the Au films was investigated by scanning electron microscopy (SEM). Figure 1(a) shows the SEM images of Au films with different average thicknesses of d = 5, 10, 15, 20, and 25 nm. Figure 1(b) highlights the linear correlation between the fractional surface coverage (p) and the average thickness. The isolated Au nanostructures coalesce into a percolating Au network above the percolation threshold coverage, p = 0.68 (d = 15 nm), in good agreement with previously reported values.[31] The Au percolation network forms more gradually here than in Au films prepared by thermal evaporation.[16,18,32]

A Ti:sapphire amplifier system (repetition rate: 1 kHz, pulse duration: 130 fs, center wavelength: 800 nm, pulse energy: 2 mJ/pulse) was employed to generate intense THz electric field transients, which were produced using a $LiNbO_3$ prism in a tilted-pulse-front
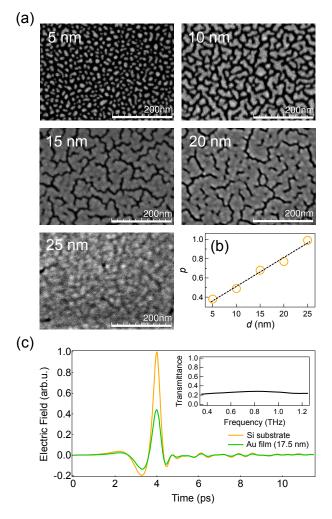

Figure 1. (a) Scanning electron micrographs of ultrathin Au films with average thicknesses of 5, 10, 15, 20, and 25 nm, sputtered on high resistivity Si substrates. (b) Fractional surface coverage of the films p as a function of their average thickness. (c) Temporal profiles of the THz electric field transmitted through either a 17.5 nm thick Au film or a plain Si substrate. The maximum field strength of the incident THz electric field was 340 kV/cm. The inset shows the power transmittance spectrum.

configuration.[2-5] The THz pulses with a beam diameter of 700 μm were incident normally on the

Au films. Peak field strengths of up to 340 kV/cm were tuned using a pair of wire-grid polarizers.

The THz wave was recorded after passing through the Au film using electro-optic (EO) sampling

with a 400-μm-thick GaP crystal. We confirmed that the transmittance of the plain Si substrate

($T_{Si} = E_{Si} / E_{air} = 0.7$) showed no variation on the incident THz field strength, ensuring that any

nonlinearities in the EO detection were negligible in our experimental condition. All the

measurements were performed at room temperature under nitrogen gas atmosphere. Figure 1(c)

compares typical THz electric-field transients transmitted thorough an Au thin film and a plain Si

substrate. The inset shows the THz transmission spectrum, $|E_{sample}(\omega)|^2 / |E_{reference}(\omega)|^2$, which is

obtained by normalizing the transmitted THz waveform from the Au thin film to that from the Si

substrate. As shown in the inset, the transmittance does not vary between 0.35 and 1.25 THz. In

the following, to discuss the dependence of the transmittance on the THz electric field strength,

the intensities are averaged over this frequency range.

Figure 2(a) shows the averaged transmittance as a function of the film thickness with different

THz peak electric fields. The averaged transmittance is almost unity below the percolation

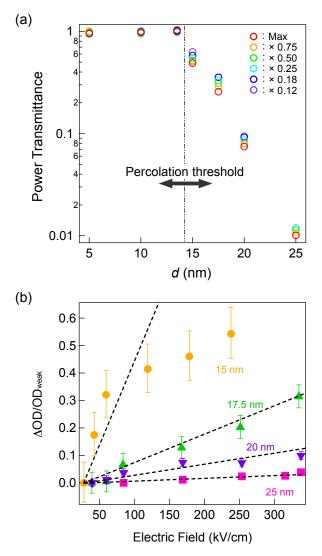threshold thickness (< 15 nm) and then decreases with increasing film thicknesses. This behavior

Figure 2. (a) Average power transmittance in the THz region as a function of film thickness

for Au films sputtered on high resistivity Si substrates, at different electric field strengths.

The vertical line indicates the percolation threshold thickness. (b) THz-field-induced

transmittance difference as a function of the electric field strength for Au films of different

thicknesses. The broken lines are guides for eyes to highlight the THz-field-induced

nonlinearity, which is more marked the steeper the line.

is typically the result of an IMT.[16] The most striking feature in Fig. 2(a) is that the transmittance decreases with increasing the THz electric field strengths, which only appears above the percolation threshold (> 15 nm). This strongly indicates that electrons in percolated Au films play a crucial role in the observed nonlinearity. To evaluate the nonlinearity, we define the THz-field-induced transmittance difference as $\Delta OD(E) / OD(E_{weak})$, where $\Delta OD(E) = OD(E) - OD(E_{weak})$, and $OD(E)$ and $OD(E_{weak})$ are respectively the average optical densities at a given THz electric field strength, E, and at the weakest field strength, E_{weak}. Figure 2(b) shows how this transmittance parameter varies as a function of the applied THz electric field strength in percolated Au nanostructures with different film thicknesses. The dashed lines, drawn to highlight nonlinear effects, show that the THz-field-induced transmittance difference depends strongly on the thickness of the film. The transmittance difference is maximal (50% more) just above the percolation threshold (~15 nm), and decreases abruptly with increasing film thicknesses, becoming negligible for the 25-nm-thick film, which is fully covered with Au ($p \approx$ 1). Note that no transmittance difference was observed for the isolated Au nanostructures, meaning that this THz-field-induced nonlinearity is characteristic of percolated Au nanostructures.

To confirm the presence of an IMT, infrared transmission spectra were measured using a conventional Fourier transform infrared (FT-IR) spectrometer. These are combined in Fig. 3(a), for various film thicknesses, with THz transmission spectra under the weakest THz electric field of 40 kV/cm. As shown in Fig. 1(a), for thicknesses below the percolation threshold (< 15 nm), the Au nanostructures are isolated so the transmittance decreases with frequency in the IR region due to a tail of localized surface plasmon resonance located at higher frequency. In the THz region, on the other hand, the film becomes transparent because of the absence of free carriers,

and therefore, behaves as an insulator. Near the percolation threshold (d = 15 nm), the transmittance becomes small at THz frequencies and the same trend is observed in the IR region, suggesting strong conduction-electron localization. In contrast, for films thicker than 20 nm, strong attenuation occurs in the THz region, but the transmittance increases with frequency in the IR region, which is typical of metallic phases.[32] This therefore verifies the presence of an IMT in our Au films.

Focusing now on THz-field-induced nonlinearity, one recalls that this is only observed for thicknesses above the percolation threshold, as shown in Figs. 2(a) and 2(b). To clarify this nonmonotonic behavior quantitatively, the sheet dielectric constant was calculated using the following formula:[7,33]

$$\tilde{\varepsilon}(\omega) = \frac{i(n_2 + 1)v_c}{\omega d} \frac{1 - T/T_0}{T/T_0}. \tag{1}$$

Here, n_2 is the dielectric constant of the Si substrate, d is the thickness of the ultrathin Au films, v_c is the velocity of light, and T/T_0 is the complex electric field transmittance of the Au films relative to that of the bare Si substrate. Figure 3(b) shows the real and imaginary parts of the dielectric constant for a 15-nm-thick Au film at the weakest field strength of 40 kV/cm. To discuss the dynamics of conduction electrons, the data were fit to the Drude-Smith model[24] using

$$\tilde{\varepsilon}(\omega) = \varepsilon_\infty - \frac{\omega_p^2}{\omega(\omega + i\gamma)}\left(1 + \frac{c}{1 - i\omega/\gamma}\right), \tag{2}$$

where ε_∞ is the dielectric constant at infinitely high frequency, ω_p is the plasma frequency, γ is the damping constant, and c $(-1 \leq c \leq 0)$ is a localization parameter that accounts for partial electron localization caused by backscattering at grain boundaries. For $c = 0$, eq. (2) reduces to the simple Drude model and gives the dielectric constant due to free electrons. Electron backscattering increases with decreasing c, and for $c = -1$, the electrons are completely localized and afford no dc conductivity. The plasma frequency can be expressed as $\omega_p = \sqrt{ne^2/(\varepsilon_0 m^*)}$, where e is the elementary charge, and n and m^* are respectively the effective density and mass of the electrons. With decreasing film thicknesses, both the effective electron density and the
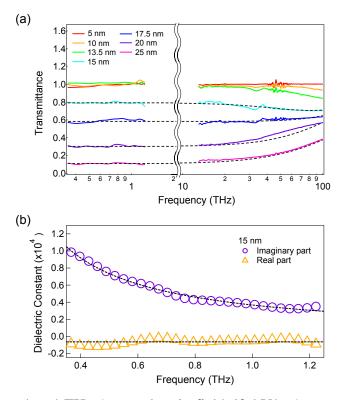

Figure 3. (a) Infrared and THz (at an electric field 40 kV/cm) transmission spectra for Au films of different thicknesses sputtered on high resistivity Si substrates. (b) Real and imaginary parts of the complex dielectric constant measured for 15 nm thick Au film. The dashed curves show the best fits obtained using the Drude-Smith model.

plasma frequency decrease because of the depolarization effect,[16,34] as confirmed by fitting the broadband transmittance data shown in Fig. 3(a). When evaluating the THz-field-induced nonlinearity, on the other hand, the plasma frequency was kept fixed at the value corresponding to the lowest electric field for all samples, because the energy of the THz pulses is far below the interband transition energy. The damping constant and the localization parameter were however kept as adjustable parameters. The resulting fits, shown in Figs. 3(a) and 3(b), have good agreement with the transmittance at 0.35–1.25 and 13–100 THz, as well as for the real and imaginary parts of the dielectric constant, ensuring that this numerical evaluation is reasonable for revealing the observed THz-field-induced nonlinear behavior.

Figures 4(a) and 4(b) show the fitted Drude-Smith parameters, the localization parameter and damping constant, as a function of the THz field strength (normalized to the maximum value), in percolated Au nanostructure films 15, 17.5, and 20 nm thick. Considering first the dependence of the Drude-Smith parameters on the film thickness at the weakest field strength, the negative localization parameter c approaches 0 as the films become thicker, whereas the damping constant decreases toward the bulk value ($\gamma / 2\pi = 17.1$ THz).[35] This indicates that thicker Au films have electromagnetic properties similar to those of bulk Au; namely, the localized electrons become mobile because of reduced backscattering at grain boundaries. Second, regarding the dependence of the Drude-Smith parameters on the field strength, although the absolute values differ between percolated Au nanostructures with different film thicknesses, in each case the damping constant decreases and the localization parameter increases toward 0 with increasing electric field strengths. This indicates that the observed nonlinearity has a single cause. Note the increased variability of the Drude-Smith parameters close to the percolation threshold thickness; the large negative value of c indicates the strong carrier backscattering due to many open gaps. The

nonlinear behavior can be understood by considering electron delocalization under strong electric field of THz pulses. We believe that electron delocalization occurs mainly through electron tunneling, which is suggested in the dc field experiments.[36] When a sufficiently strong local field is applied to a nanometer-scale insulating bridge, the insulating channel becomes conductive due to inter-grain tunneling, leading to less electron backscattering and thereby lowering the damping constant. Note that the characteristic time required to complete the electron tunneling is sufficiently short compared with the oscillation period of the THz electric field (~1 ps).[37] The THz electric field is therefore regarded as a quasi-static field for the tunneling process, and as a result, it could effectively produce the nonlinearity.

Note finally that this nonlinear response is repeatable, not irreversible—as is for instance material breakdown.[38] The reversibility was confirmed by the THz transmission measurement with low field strength after intense THz irradiations. Any irreversible change was observed in
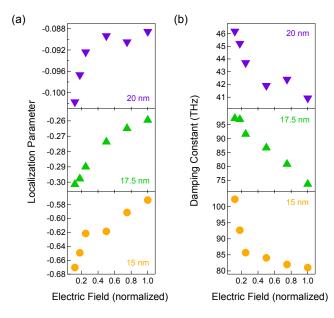

Figure 4. (a) The localization parameter and (b) the damping constant in the Drude-Smith model as a function of the normalized THz field strength for Au films with different average thicknesses.

our ultrathin Au films. In micrometer-scale metamaterials with Au split-ring resonators (SRR), strong electric field enhancement occurs at THz frequencies due to LC resonance.[10] This THz-electric-field enhancement can readily and permanently damage SRR gap structures. On the contrary, the percolated Au nanostructures are not damaged, probably because the electron tunneling itself reduces the field enhancement[20] and/or the relatively long length-scale of the Au network places their resonance outside the THz range. Percolated Au nanostructures therefore suppress excess THz-field enhancement and avoid permanent breakdown, while retaining the nonlinearity required to enhance electron tunneling across the nanometer-scale insulating bridges. Our findings—large THz-field-induced opacity and/or nonlinear electron delocalization in percolated Au nanostructures—should prove useful for controlling and enhancing the unique electromagnetic properties of metal nanostructures on the picosecond timescale, which more generally, will be useful for future microelectronics and nanometer-scale plasmonic devices.[39,40]

In conclusion, the nonlinear response of localized electrons driven by intense THz electric field transients has been demonstrated in ultrathin Au films with percolated Au nanostructures. As the THz electric field strength is increased, large opacity in the THz transmission spectrum takes place in percolated Au nanostructures. The Drude-Smith model was applied over wide frequency ranges, viz. 0.35–1.25 and 13–100 THz, to understand the nonlinear behavior of localized electrons quantitatively. The damping constant in this model decreases and the localization parameter increases as the strength of the incident THz electric field is increased. The experimental data indicate that ultrafast electron delocalization occurs due to strong electric field of THz pulses, leading to electron tunneling across the narrow insulating bridge between Au nanostructures without material breakdown. These results show that intense THz pulses are a unique means of controlling the electromagnetic properties of metal nanostructures. Further

investigations with well-aligned Au nanostructures and detailed analysis are needed to fully understand the electron delocalization mechanism.

AUTHOR INFORMATION

Corresponding Authors

*E-mail: jun@ynu.ac.jp; minamiyasuo@ynu.ac.jp; katayama@ynu.ac.jp.

Author Contributions

All authors contributed to writing the manuscript and have approved its final version.

Notes

The authors declare no competing financial interests.

ACKNOWLEDGMENT

REFERENCES

(1) Hebling, J.; Yeh, K.-L.; Hoffmann, M.C.; Nelson, K. A. *IEEE J. Sel. Top. Quantum Electron.* **2008**, *14*, 345–353.

(2) Fülöp, J. A.; Pálfalvi, L.; Almási, G.; Hebling, J. *Opt. Express* **2010**, *18*, 12311–12327.

(3) Hirori, H.; Doi, A.; Blanchard, F.; Tanaka, K. *Appl. Phys. Lett.* **2011**, *98*, 091106.

(4) Jewariya, M.; Nagai, M.; Tanaka, K. *J. Opt. Soc. Am. B* **2009**, *26*, A101–A106.

(5) Blanchard, F.; Ropagnol, X.; Hafez, H.; Razavipour, H.; Bolduc, M.; Morandotti, R.; Ozaki, T.; Cooke, D. G. *Opt. Lett.* **2014**, *39*, 4333–4336.

(6) Minami, Y.; Kurihara, T.; Yamaguchi, K.; Nakajima, M.; Suemoto, T. *Appl. Phys. Lett.* **2013**, *102*, 041105.

(7) Katayama, I.; Aoki, H.; Takeda, J.; Shimosato, H.; Ashida, M.; Kinjo, R.; Kawayama, I.; Tonouchi, M.; Nagai, M.; Tanaka, K. *Phys. Rev. Lett.* **2012**, *108*, 097401.

(8) Miyamoto, T.; Yada, H.; Yamakawa, H.; Okamoto, H. *Nat. Commun.* **2013**, *4*, 2586–2594.

(9) Somma, C.; Reimann, K.; Flytzanis, C.; Elsaesser, T.; Woerner, M. *Phys. Rev. Lett.* **2014**, *112*, 146602.

(10) Liu, M.; Hwang, H. Y.; Tao, H.; Strikwerda, A. C.; Fan, K.; Keiser, G. R.; Sternbach, A. J.; West, K. G.; Kittiwatanakul, S.; Lu, J.; Wolf, S. A.; Omenetto, F. G.; Zhang, X.; Nelson, K. A.; Averitt, R. D. *Nature* **2012**, *487*, 345–348.

(11) Junginger, F.; Mayer, B.; Schmidt, C.; Schubert, O.; Mährlein, S.; Leitenstorfer, A.; Huber, R.; Pashkin, A. *Phys. Rev. Lett.* **2012**, *109*, 147403.

(12) Schubert, O.; Hohenleutner, M.; Langer, F.; Urbanek, B.; Lange, C.; Huttner, U.; Golde, D.; Meier, T.; Kira, M.; Koch, S. W.; Huber, R. *Nat. Photon.* **2014**, *8*, 119–123.

(13) Tani, S.; Blanchard, F.; Tanaka, K. *Phys. Rev. Lett.* **2012**, *109*, 166603.

(14) Hwang, H. Y.; Brandt, N. C.; Farhat, H.; Hsu, A. L.; Kong, J.; Nelson, K. A. *J. Phys. Chem. B.* **2013**, *117*, 15819–15824.

(15) Tu, J. J.; Homes, C. C.; Strongin, M. *Phys. Rev. Lett.* **2003**, *90*, 017402.

(16) Walther, M.; Cooke, D. G.; Sherstan, C.; Hajar, M.; Freeman, M. R.; Hegmann, F. A. *Phys. Rev. B* **2007**, *76*, 125408.

(17) Hoang, C. V.; Oyama, M.; Saito, O.; Aono, M.; Nagao, T. *Sci. Rep.* **2013**, *3*, 1175–1180.

(18) Ramakrishnan, G.; Planken, P. C. M. *Opt.Lett.* **2011**, *36*, 2572–2574.

(19) Tripathi, V.; Loh, Y. L. *Phys. Rev. B* **2006**, *73*, 195113.

(20) J. W. Haus, D. Ceglia, M. A. Vincenti, and M. Scalora, *J. Opt. Soc. Am. B* **2014**, *31*, 259–269.

(21) Garnett, J. C. M. *Philos. Trans. R. Soc. London. Ser. A* **1904**, *203*, 385–420.

(22) Bruggeman, D. A. G. *Ann. Phys.* **1935**, *416*, 636–664.

(23) Němec, H.; Kužel, P.; Sundström, V. *Phys. Rev. B* **2009**, *79*, 115309.

(24) Smith, N. V. *Phys. Rev. B* **2001**, *64*, 155106.

(25) Lovrinčić, R.; Pucci, A. *Phys. Rev. B* **2009**, *80*, 205404.

(26) Richter, C.; Schmuttenmaer, C. A. *Nat. Nanotechnol.* **2010**, *5*, 769–772.

(27) Cooke, D. G.; Krebs, F. C.; Jepsen, P. U. *Phys. Rev. Lett.* **2012**, *108*, 056603.

(28) Jensen, S. A.; Ulbricht, R.; Narita, A.; Feng, X.; M üllen, K.; Hertel, T.; Turchinovich, D.; Bonn, M. *Nano Lett.* **2013**, *13*, 5925－5930.

(29) Al-Bayati, A. H.; Ormannn-Rossiter, K. G.; van den Berg, J. A.; Armour, D. G. *Surf. Sci.* **1991**, *241*, 91–102

(30) Wen, H.; Wiczer, M.; Lindenberg, A. M. *Phys. Rev. B* **2008**, *78*, 125203.

(31) Yagil, Y.; Gadenne, P.; Julien, C.; Deutscher, G. *Phys. Rev. B* **1992**, *46*, 2503–2511.

(32) Gompf, B.; Beister, J.; Brandt, T.; Pflaum, J.; Dressel, M. *Opt. Lett.* **2007**, *32*, 1578−1580.

(33) Yokota, K.; Takeda, J.; Dang, C.; Han, G.; McCarthy, D. N.; Nagao, T.; Hishita, S.; Kitajima, M.; Katayama, I. *Appl. Phys. Lett.* **2012**, *100*, 251605
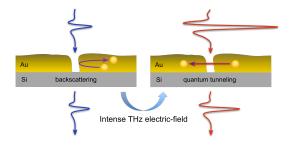
(34) Bittar, A.; Berthier, S.; Lafait, J. *J. Phys. (Paris)* **1984**, *45*, 623−631.

(35) Johnson, P.B.; Christy, R.W. *Phys. Rev. B* **1972**, *6*, 4370−4379.

(36) Gefen, Y.; Shih, W.; Laibowitz, R.B.; Viggiano, J.M. *Phys. Rev. Lett.* **1986**, *57*, 3097–3100.

(37) Shafir, D.; Soifer, H.; Bruner, B. D.; Dagan, M.; Mairesse, Y.; Patchkovskii, S.; Ivanov, M. Y.; Smirnova, O.; Dudovich, N. *Nature* **2012**, *485*, 343−346.

(38) Yagil, Y.; Deutsher, G.; Bergman, D. *J. Phys. Rev. Lett.* **1992**, *69*, 1423–1426.

(39) Scholl, J. A.; García-Etxarri, A.; Koh, A. L.; Dionne, J. A. *Nano Lett.* **2013**, *13*, 564−569.

(40) Gao, W.; Shu, J.; Reichel, K.; Nickel, D. V.; He, X.; Shi, G.; Vajtai, R.; Ajayan, P. M.; Kono, J.; Mittleman, D. M.; Xu, Q. *Nano Lett.* **2014**, *14*, 1242−1248.

Insert Table of Contents Graphic and Synopsis Here.